

Investigation of UV/TiO₂-N photocatalytic degradation of AR 40 using response surface methodology (RSM)

Mohsen Nademi^{1*}, Mostafa Keshavarz Moraveji², Mohsen Mansouri³

1. Department of Chemical Engineering, Islamic Azad University, Tehran North Branch, Tehran, Iran
2. Department of Chemical Engineering, Amirkabir University of Technology (Tehran Polytechnic), Tehran, Iran
3. Department of Chemical Engineering, Ilam University, Ilam, Iran

***Corresponding author:** Tel: +98 9183444260 Fax: +98 8432227026

Address: Department of Chemical Engineering, Islamic Azad University, Tehran North Branch, Tehran, Iran

E-mail: mohsen.nademi@yahoo.com

Received; 2016/06/1 revised; 2016/07/19 accepted; 2016/08/4

Abstract

Introduction: Advanced oxidation processes (AOPs) suggest a highly reactive, nonspecific oxidant namely hydroxyl radical (OH•), that oxidize a wide range of pollutants fast and non-selective in wastewater and water.

Materials and methods: In this work, the nitrogen-doped titanium dioxide nanoparticles were primed by sol-gel method, characterized by X-ray diffraction and Scanning Electron Microscopy (SEM), for the degradation of Acid Red 40 (AR 40) solution in water. The effectiveness of the treatment method applied for the degradation of AR 40 based on AOPs was investigated.

Results: The three various key parameters were optimized by using response surface modeling, namely: pH, TiO₂-N concentration and the initial AR 40 concentrations. The optimized values were obtained at pH = 11, TiO₂-N concentration = 0.09 g/L, and the initial AR 40 concentration = 19 mg/L.

Conclusion: Under the optimum conditions, performance of photocatalytic degradation reaches 92.47% in 1 hr. Kinetic constant was evaluated using first-order equation to obtain the rate constant, K.

Keywords: Photocatalytic degradation, AR 40, TiO₂-N nanoparticles, Response surface modeling

Introduction

Around four Billion of people throughout the world cannot access to sound water or have a little access to safe water (1). This statistical result may increase the amount of polluted water in the near future because of excess destruction contaminations and micro contaminations. The necessity for using of effective operations of removal and separation is necessary because of concern for water environment contaminations (2). Most common methods such as physical (like absorbance), biological, chemical methods

and combination of these methods were used in refining of polluted wastewater, so far. Common processes are not appropriate for refining of these wastewaters because these kind of methods causes a defect destruction of contamination and just transfer from one phase to another phase as well as we have a second contamination. As a result, applying chemical processes based on Oxidation Process has been considered. Since most contaminations that exist in environment belong to organic components that are

deconstructed by Oxidation Process. Therefore, in these kinds of methods, strong oxidations like H_2O_2 and O_3 are used. Of course, composition such as O_3 is dangerous and excess using of these kinds of Oxidations results in polluted environments. Researchers in order to improve the process of degradation of contamination, try to use Advanced Oxidation Process (AOPs) (3). In the last three decades, advanced oxidation processes have been an efficient method for degradation of organic contaminants. One of the AOPs is the photocatalysis process that mineralizes and degrades the organic contaminants (4). Advanced Oxidation Process is widely used for photocatalytic degradation of organic contaminants in water and air because of its non-soluble, non-toxic, high photocatalytic activity, doable in low pressure and in low temperature and low production cost (5-8). Many researchers have done the photocatalytic degradation by using TiO_2 and metal-doped TiO_2 either in powder or in thin film form (9-12). One of the main problems in using the pure TiO_2 is re-combination between electron and hole. For finding a solution, several studies such as metal or nonmetal iron doping have been done to improve photocatalytic efficiency of TiO_2 (5-8).

Technical advance related to progress of photocatalytic process has not been done completely. Various parameters in this system should be considered and evaluated. One of obstacles in this direction to use Advanced Oxidation Process in large scale is that in previous works One-factor-at-a-time (OFAT) was widely used (13-16). If the variables of process are independent, however that is less likely to happen; common method is One-factor-at-a-time (17). If this method is used, the checking between variables of operation process is not possible. In addition, considering indicates that this method is a time-consuming way and expensive method related to consuming chemical material (17). Recently, many

tries have been done to substitute more effective way such as Response Surface Methodology (RSM) for One-factor-at-a-time method. This method has been established based on analysis, statistical explanation, and experimental design is a good strategy to determine the optimal condition in multiple variables systems.

In this study, TiO_2 and $\text{TiO}_2\text{-N}$ nanoparticles were synthesized by sol-gel method, and then characterized by X-ray diffraction (XRD), and scanning electron microscope (SEM). After this procedure, the effects of parameters such as solution's initial pH, the temperature of solution, $\text{TiO}_2\text{-N}$ and contaminant's concentration on photo catalytic degradation were examined. Finally, the cost analysis was evaluated.

Materials and methods

Materials: For the purpose of synthesis, hydroxyl propyl cellulose (HPC), titanium tetraisopropoxide (TTIP), acetic acid, pure alcohol, 1,3-diaminopropane, di-ethanol amine, ethanol amine, NaOH and H_2SO_4 —all in analytical grade—are purchased from Merck Company. The Acid Red 40 is gifted by Alvansabet Co. Iran.

Instruments: To determine nanoparticles' structure, XRD (Philips PW 1800) was employed. To specify the nanoparticles' surface morphology, SEM (Leo 1455 VP) was applied. UV/Vis spectrophotometer (CECIL 2501) was used for determination of Acid Red 40's concentration.

Preparation of photocatalyst: At the first, each part of $\text{TiO}_2\text{-N}$ nanocomposite was prepared separately before mixing by sol-gel method. In the following, the method of constructing of each component of nanocomposite will explain.

For preparing of TiO_2 , initially hydroxyl propyl cellulose (HPC) was solved in ethanol under quick stirring for five minutes. Then, titanium tetraisopropoxide (TTIP) was added to the previous mixture and was stirring for fifteen minutes. After that, the mixture of glacial acetic acid, pure alcohol and deionized water was

added to previous mixture. It was stirred for fifteen minutes just to make sure for a yellow transparent acidic TiO₂ sol. The sol was kept at room temperature for thirty minutes.

The second component of nanocomposite is N. First, 1,3-diaminopropane was dissolved in pure alcohol and was stirred for five minutes. Then the mixture of di-ethanol amine, pure alcohol, and deionized water was added to solution under vigorous constant stirring condition. The solution was constantly stirred for fifteen minutes to reach a transparent sol N.

Finally, the sol of N was mixed directly with the sol of TiO₂ to prepare the TiO₂-N nanocomposite. That nanocomposite was dried at room temperature. Then, the nanocomposite sintered at the temperature of 350 °C for 10 minutes and after that, sintered at the temperature of 500 °C for five hours in order to calcinate (the temperature was being increased five Celsius per second) and finally, the catalyst was prepared (18).

Experimental: All photochemical reactions for degradation of Acid Red 40 with TiO₂-N were carried out in a batch reactor, which was made from cylindrical glass with one liter in volume. The reaction mixture in the reactor circulates in the closed cycle between pump and reactor. In addition, reactions' temperature was monitored. A 15 W lamp from the Phillips emitting UV light of wavelength 254 nm, which was immersed in the solution, was applied to serve the UV radiation in the reactor. The volume of the reaction mixture for each of the tests which proposed by RSM experimental design was 1000 cc. In the end, to analyze the concentration of Acid Red 40, 3 cc of the solution inside the reactor was taken out after 90 min and analyzed for decolorization of AR 40 after centrifugation.

Analysis: Color removal was evaluated by UV/Vis spectrophotometer (CECIL2501) at the λ_{\max} value of 530 nm

for Acid Red 40. The color removal was determined using Equation (1).

Dye removal (%) = $(C_0 - C_t) / C_0 \times 100$ (1)
where, C_0 is the initial concentration of AR 40 in ppm and C_t is Acid Red 40's concentration based on ppm at any time t.

Experimental design: Initially preliminary experiments were conducted using single factor study method to identify the significant experimental parameters affecting the photocatalytic AR 40 treatment. The selected factors were catalytic dose, initial concentration of AR 40, temperature and pH of the reaction mixture.

The three selected experimental parameters were optimized by RSM as the independent variables and the percentage of degradation of AR 40 as the response variables. Central composite design of experiments is employed to examine the combined effects of the four independent variables on the response through 17 sets of experiment. The ranges and levels of the independent variables are shown in Table 1. This design along with RSM has been widely used to optimize various physical, chemical and biological processes (19-22). By using RSM, the results are matched to an empirical quadratic polynomial model for the four parameters expressed in the Equation (2):

$$Y = \beta_0 + \beta_1A + \beta_2B + \beta_3C + \beta_{11}A^2 + \beta_{22}B^2 + \beta_{33}C^2 + \beta_{12}AB + \beta_{23}BC + \beta_{13}AC \quad (2)$$

Where, Y denotes the response variable, β_0 the intercept, $\beta_1, \beta_2, \beta_3$ the coefficients of the independent variables, $\beta_{11}, \beta_{22}, \beta_{33}$ quadratic coefficients, $\beta_{12}, \beta_{23}, \beta_{13}$ the interaction coefficients and A, B, C are the independent variables. Multivariate regression analysis and optimization process were performed by means of RSM and using Design Expert software (version 7, Stat Ease Inc., USA). The obtained values from analysis of variance (ANOVA) were found significant at $p < 0.05$. The optimum values for the independent variables were found using three-dimensional response surface analysis of the independent and dependent

variables. The designed experiments and the experimental and predicted values of the response were detailed in Table 2. Also, the variations were shown in Figure 1d. The effect of the independents variable on the decolorization were shown in Figure 1 (a,b,c).

Results

X-ray diffraction and SEM: The nanoparticles' structure of TiO₂-N was specified by using X-ray diffraction (XRD). Figure 2 represents the XRD patterns of the prepared TiO₂-N and TiO₂ nanoparticles. As it is shown in Figure 2, that all peaks are found at 25.36°, 38.18°,

48.09°, 53.75° and 62.36° for TiO₂; and 25.38°, 27.42°, 36.98°, 49.97°, 55.56° and 63.53° for TiO₂-N. It is shown that the 2-theta values of X-ray patterns of TiO₂ and TiO₂-N consistent with anatase for both of them. The XRD patterns illustrate that the composition of TiO₂-N does not alter the catalyst structure of TiO₂. This may be due the fact that the concentration of nitrogen in the composition was low. The particle size of the samples can be calculated by Debye-Scherrer formula:

$$D = \frac{K\lambda}{\beta \cos \theta} \quad (3)$$

Table 1. The levels and ranges of variables in Central-Composite statistical experiment design.

Factors	-α	-1	0	1	α
Dye amount (mg/L)	5	10	15	20	25
Catalyst amount (g/L)	0.03	0.06	0.09	0.12	0.15
pH	3	5	7	9	11

Table 2. Central-Composite experiments along with actual and predicted values of responses.

Std	Run	Initial dye concentration (mg/L)	Catalyst loading (g/L)	pH	Dye removal (%)	
					Actual	Predicted
1	12	10	0.06	5	58.41	63.50
2	1	20	0.06	5	64.50	60.68
3	3	10	0.12	5	74.17	74.07
4	14	20	0.12	5	46.04	55.08
5	2	10	0.06	9	76.92	70.35
6	4	20	0.06	9	74.11	76.68
7	13	10	0.12	9	71.22	77.52
8	6	20	0.12	9	70.30	67.68
9	7	5	0.09	7	63.72	62.59
10	16	25	0.09	7	51.29	49.93
11	8	15	0.03	7	59.169	61.76
12	15	15	0.15	7	68.41	63.33
13	5	15	0.09	3	75.38	71.51
14	9	15	0.09	11	89.56	90.96
15	11	15	0.09	7	75.62	72.75
16	10	15	0.09	7	72.07	72.75
17	17	15	0.09	7	73.02	72.75

In Equation (1), D is the average crystal size (nm), K is the Scherrer constant, a arbitrary value that falls within the range 0.8-1.0 (it is assumed to be 0.9 in the present study), λ is wavelength of X-ray

radiation (0.154 nm), θ is the diffraction angle and β is full width at half maximum (FWHM). The particle size calculated value for TiO₂ and TiO₂-N nanoparticles is 12.81 nm and 12.76 nm, respectively.

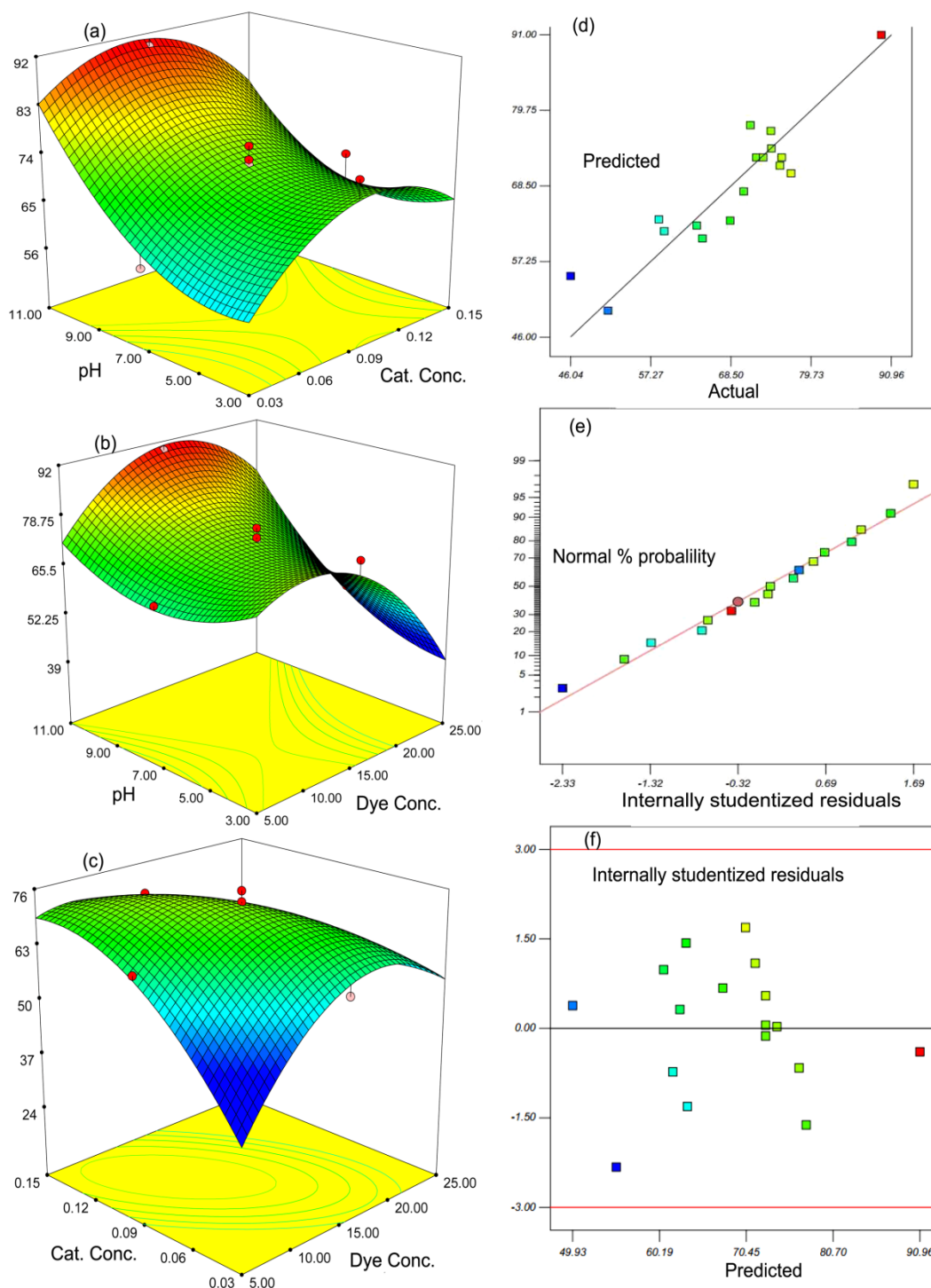


Figure 1. Effects of catalyst loading, initial dye, and pH on decolorization of AR 40.

Table 3. The effect of different lamps on kinetic constant and E_{EO} at dye removal optimum conditions.

UV lamp (W)	K_{app} (min^{-1})	E_{EO} ($\text{kW} \cdot \text{m}^{-3} \cdot \text{min}^{-1}$)
5	0.0059	32542.372
15	0.0395	14582.278
25	0.0471	20382.165

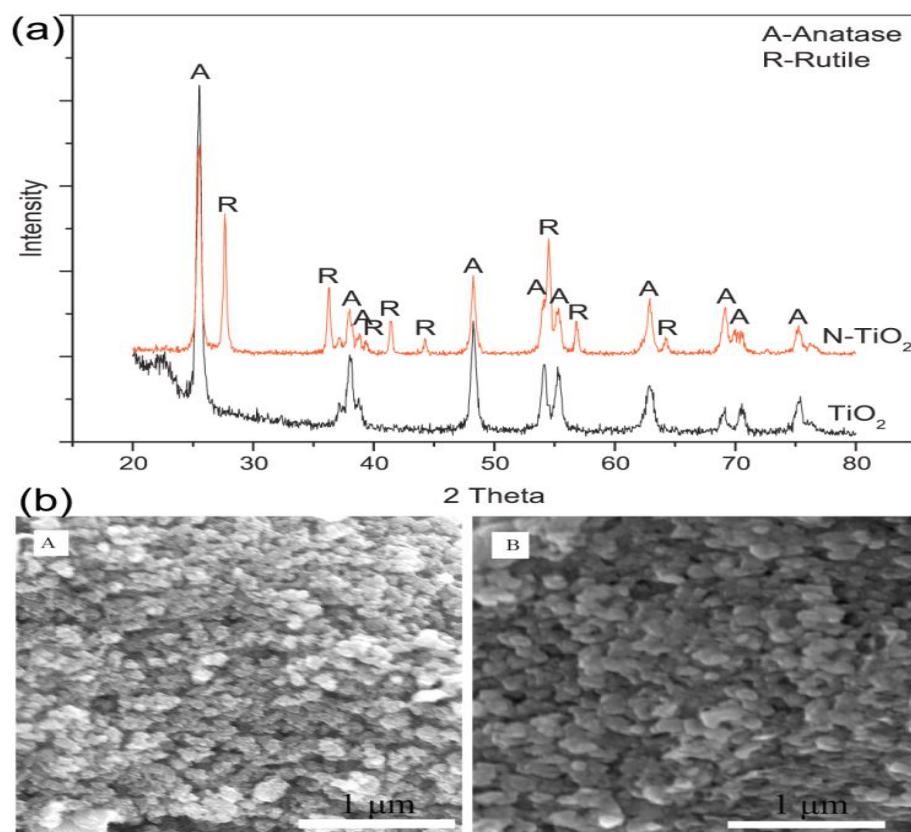


Figure 2. Catalyst characterization (a) XRD pattern of TiO_2 and $\text{TiO}_2\text{-N}$ nanocatalysts, (b) SEM image of (A) TiO_2 and (B) $\text{TiO}_2\text{-N}$ nanocatalysts.

The sample's surface morphology was tested by scanning electron microscope (SEM). SEM image TiO_2 and $\text{TiO}_2\text{-N}$ nanoparticles is shown in Figure 2. This figure represents that sphere-shaped particles are formed in good resemblance to each other. As SEM Images show, the average particle size of $\text{TiO}_2\text{-N}$ nanoparticles is approximately 13.75 nm. Further, it can be observed that the crystal size evaluated by XRD differs from the obtained results by SEM. This difference can be due to the fact that an XRD pattern gives the crystal size of a particle, whereas a SEM image gives the particle size itself which is the aggregation of several crystals (23-25).

Optimization of removal conditions using RSM: To gain a suitable model, tests of significance for the regression model and for each coefficient of the model as well as the test for lack-of-fit ought to be conducted.

The R-square is found to be 0.8399, which is close to 1 and significant, implying that about 83.44 % of changes in the data can be explained by the model. Adequate accuracy compares the range of the estimated value at design points with the mean prediction error. The ratios greater than 4 indicate the model's adequate discrimination power. The result of the above comparison is found to be greater than 4, implying the model's adequate discrimination power. The lack-of-fit P value of 0.0386 suggests the lack-of-fit is not significant relative to net error; this is suitable, since we look for a model that matches.

Following the experimental design (Table 2), empirical second order polynomial equations are developed for the percentage of degradation of AR 40 in terms of the four independent variables as it is expressed in Equation (4).

$$\text{Dye removal (\%)} = 72.75 - 3.17 A + 0.39 B + 4.86 C - 4.12 A^2 - 2.55 B^2 + 2.12 C^2 - 4.04 AB - 0.85 BC + 2.29 AC \quad (4)$$

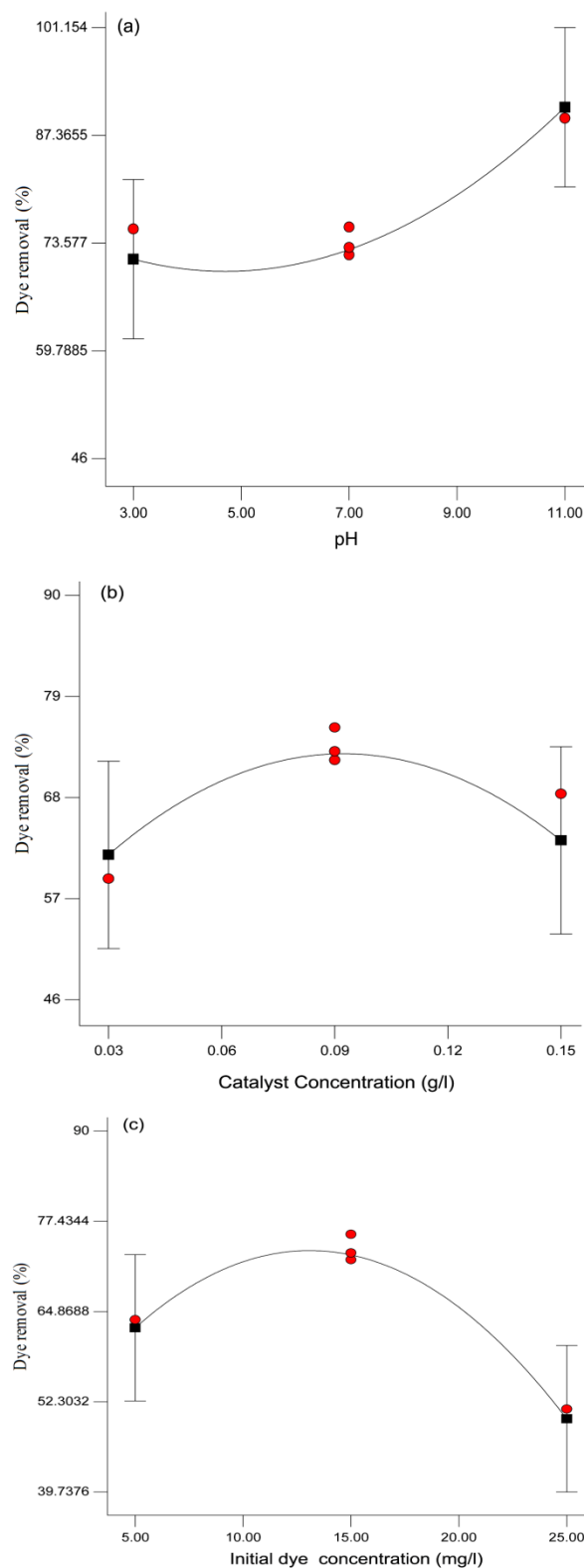


Figure 3. Effect of pH, catalytic dose, and initial dye concentration on dye removal (%) (a) catalytic dose = 0.09 (g/l), initial dye concentration = 15 (mg/l); (b) pH = 7, initial dye concentration = 15 (mg/l); (c) catalytic dose = 0.09 (g/l), pH = 7.

The experimental data for degradation of AR 40 was statistically analyzed by using ANOVA. The ANOVA of the second order polynomial model (F-value = 4.08, p-value < 0.0001) shows that the model is significant, i.e. there is only a chance of 0.01% for occurrence of the model's F-value due to the noise. The normal probability plot (Scatter Diagram) for the studentized residuals is presented in Figure 1e. The points on this plot lie reasonably close to the straight line, confirming that the errors have normal distribution with a zero mean and a constant. The curvature P-value < 0.0001 indicates that there is a significant curvature (as measured by the difference between the mean center points and the mean factorial points) in the design space. Consequently, a linear model along with the interaction terms giving a twisted plane was not adequate to explain the response. Besides, plots of the residuals in Figure 1f reveal that they have no obvious pattern and their structure is rather abnormal. Moreover, they indicate equal scatter above and below the x-axis, implying the proposed model's adequacy, so there is no reason to suspect any violation.

Discussion

Effect of Initial pH on the photocatalysis of AR 40: pH is one of the most important parameters in photocatalytic degradation of organic contaminants. The effect of pH on the photocatalytic degradation of Acid Red 40 was appraised with the initial pH at three various ranges of 3 - 11, as it is represented in Figure 3a. The degradation of Acid Red 40 lessens as the pH value increases from 3 to 11. The pH of the solution has complicated effects on the photocatalytic oxidation reaction. Generally, the pH effect relies on the type of contamination and zero point charge (ZPC) of semiconductor (catalyst) in the oxidation process. The phenomenon can be illustrated in terms of the location of the point of zero charge (isoelectric point) of

the $\text{TiO}_2\text{-N}$. It can be concluded that the photodegradation of Acid Red 40 is much greater at alkalinity pH than in neutral/alkaline solutions.

Effect of $\text{TiO}_2\text{-N}$ concentration on the photocatalysis of AR 40: The experiments were accomplished to examine the effect of catalyst loading on photocatalytic degradation Acid Red 40 under conditions 0.03 - 0.15 g/l. Figure 3b indicates the percentage of degradation efficiency versus catalyst loading for several initial $\text{TiO}_2\text{-N}$ nonparticles' concentrations. The percentage of degradation efficiency augments as the catalyst loading raises from 0.03 to 0.15 g/L. However, by an increase in excess of 0.09 g/l, this percentage goes down. It should be noted that these results are highly likely to the maintained experimental conditions. As the amount of catalyst raise, the number of adsorbed photons and molecules raise as well due to a growth in the number of $\text{TiO}_2\text{-N}$ nanoparticles. As a result, the particles' density within the illumination area increases. (26) This behavior can be attributed that some photocatalyst particles may not receive enough energy to produce hydroxyl radical and start Acid Red 40 oxidation (19). It may also result from $\text{TiO}_2\text{-N}$ aggregation, increasing obscurity, reducing the active points on its surface to adsorb organic compounds and UV, thereby reducing the quantity of $e\text{-}h^+$ and OH free radicals and affecting the degradation (26-29).

Effect of initial concentration of dye on the photocatalysis of AR 40: Increasing of initial concentration of Acid Red 40 reduces its degradation as it is shown in Figure 3c. Similar results have been reported on the photocatalytic oxidation of other organic compounds interface (29-31). Thus, at low concentration Acid Red 40, a larger number of water molecules will be adsorbed onto the available $\text{TiO}_2\text{-N}$ particles, producing hydroxyl radicals and leading to a rapid oxidation process. On the other hand, at high concentration of

Acid Red 40, there is a smaller portion of water molecules to free active sites, since the number of active sites remains the same. Consequently, competition between the Acid Red 40 and water molecules on adsorption intensifies, leading to decline in the degradation rate.

Photocatalytic reaction kinetic: Kinetics of photocatalytic degradation of the Acid Red 40 was examined based on optimum conditions which were obtained from previous sections at catalyst concentration of 0.09 g/L and pH = 11 in light intensity of 15 W UV-V.

Generally, first-order kinetics is appropriate for photocatalytic reactions (31-32). Kinetics model as follows:

$$-r_A = -\frac{dC}{dt} = KC \quad (5)$$

After integration of Equation (6), the following equation is obtained:

$$\ln\left(\frac{C_0}{C}\right) = Kt \quad (6)$$

where r_A is the oxidation rate of the Acid Red 40 ($ppm(\min^{-1})$), K the apparent constant of the reaction rate (the constant of first order reaction), C the concentration of the Acid Red 40 (ppm), C_0 the initial concentration of Acid Red 40, t the time required for the initial concentration of Acid Red 40 C_0 to become C (min).

The rate constant of $0.0395 \min^{-1}$ was estimated from the slope of $\ln(C/C_0)$ vs. time, plotted under optimized conditions.

Evaluation of economic of degradation process: Some paramount parameters that have effects on technology of effluents treatment to be chose includes: economic, rule and law of environmental quality of refined final effluents. Usually, economical parameter is more important, although all those parameters are vital. As a result, electrical energy per mass (E_{EM}) is the amount of electrical energy that is used to degrade one kilogram of contamination.

Electrical energy per mass (E_{EM}) in regard to first-order kinetics is the amount of energy which is applied to destroy 90 percent of contamination in one thousand liters of polluted water. Electrical energy per mass (E_{EM}) is defined as follow:

$$E_{(EO)} = (P \times t \times 1000) / (V \times 60 \times \log(C_0/C)) \quad (7)$$

Where P is power of lamp (kW) which is applied for advanced degradation system, t time of radiation (minute), V the volume of contamination in reactor (m^3), C_0 initial concentration of Acid Red 40, C final concentration of Acid Red 40, and K constant rate of first-order reaction (\min^{-1}). Equation (8) is obtained by combination of Equations (6) and (7).

$$E_{(EO)} = (P \times 38.4) / (V \times K) \quad (8)$$

The amount of consuming electrical energy is calculated for different lamps that were applied in photocatalytic degradation in this study under optimum conditions that were obtained in pervious sections. Those are shown in the Table 3. It can be seen that the 15 W lamp has the best efficiency (lower $E_{(EO)}$) in regard to consumption of electricity in comparison with 5 W and 20 W lamps.

Conclusion

In this study, TiO_2 -N nanoparticles synthesized by sol-gel method are used as the catalyst to photocatalytic degradation of Acid Red 40. The crystal size of TiO_2 -N is 12.76 nm that is calculated by Debye-Scherrer formula. The optimal operation parameters are found by RSM method at pH of 11, TiO_2 -N concentration of 0.09 g/L, and initial concentration of 19 mg/L in solution's temperature. Under the optimum conditions, performance of photocatalytic degradation reaches 92.47% in 1 hour. The economical parameter is appraised which the light intensity 15 W UV-V has the lowest consumption of electricity in comparison with 5 W and 20 W lamps.

References

1. Chong MN, Jin B, Chow CWK, Saint C. Recent developments in photocatalytic water treatment technology: A review. *Water Res.* 2010; 44(10): 2997-3027.
2. Shan AY, Ghazi TIM, Rashid, SA. Immobilisation of titanium dioxide on to supporting materials in heterogeneous photocatalysis: A review. *Appl Catal A Gen.* 2010; 389(1-2): 1-8.
3. Rajeshwar K, Osugi ME, Chanmanee W, Chenthamarakshan CR, Zaroni MWB, Kajitvichyanukul P, Krishnan-Ayer R. Heterogeneous photocatalytic treatment of organic dyes in air and aqueous media. *J Photochem Photobiol C Photochem Reviews.* 2008; 9(4): 171-92.
4. Arana J, Peña Alonso A, Doña Rodríguez JM, Herrera Melián JA, González Díaz O, Pérez Peña J. Comparative study of MTBE photocatalytic degradation with TiO₂ and Cu-TiO₂. *Appl Catal B* 2008; 7(8): 355-63.
5. Colon G, Maicu M, Hidalgo MS, Navio JA. Cu-doped TiO₂ systems with improved photocatalytic activity. *Appl Catal B Environ.* 2006; 67(1): 41-51.
6. Liqiang J, Hongganga F, Baiqia W, Dejunb W, Baifua X, Shudana L, Jiazhong S. Effects of Sn dopant on the photoinduced charge property and photocatalytic activity of TiO₂ nanoparticles. *Appl Catal B.* 2006; 6(2): 282-91.
7. Chang SM, Doong RA. Characterization of Zr-doped TiO₂ nanocrystals prepared by a nonhydrolytic sol-gel method at high temperatures. *J Phys Chem B.* 2006; 110(42): 20808-14.
8. Luo H, Takata T, Lee Y, Zhao J, Domen K, Yan Y. Photocatalytic activity enhancing for titanium dioxide by co-doping with bromine and chlorine. *Chem Mater.* 2004; 16(5): 846-9.
9. Vinu R, Madras G. Synthesis and photoactivity of Pd substituted nano TiO₂. *J Mol Catal A Chem.* 2008; 291(1): 5-11.
10. Sahoo C, Gupta AK, Pal A. Photocatalytic degradation of Methyl Red dye in aqueous solutions under UV irradiation using Ag doped TiO₂. *Desalination.* 2005; 181(1-3): 91-100.
11. Naskar S, Pillay SA, Chanda M. Photocatalytic degradation of organic dyes in aqueous solution with TiO₂ nanoparticles immobilized on foamed polyethylene sheet. *J Photochem Photobiol A Chem.* 1998; 113(3): 257-64.
12. Gupta VK, Jain R, Mittal A, Saleh TA, Nayak A, Agarwal S, Sikarwar S. Photo-catalytic degradation of toxic dye amaranth on TiO₂/UV in aqueous suspensions. *Mater Sci Eng C.* 2012; 32(1): 12-7.
13. Ochuma IJ, Fishwick RP, Wood J, Winterbottom JM. Optimisation of degradation conditions of 1,8-diazabicyclo[5.4.0]undec-7-ene in water and reaction kinetics analysis using a concurrent down flow contactor photocatalytic reactor. *Appl Catal B Environ.* 2007; 73(3-4): 259-68.
14. Bhargava, A., Kabir MF, Vaisman E, Langford CH, Kantzas A. Novel technique to characterize the hydrodynamics and analyze the performance of a fluidized-bed photocatalytic reactor for wastewater treatment. *Ind Eng Chem Res.* 2004; 43(4): 980-9.
15. Toor AP, Verma A, Jotshi CK, Bajpai PK, Singh V. Photocatalytic degradation of Direct Yellow 12 dye using UV/TiO₂ in a shallow pond slurry reactor. *Dyes and Pigments.* 2006; 68(1): 53-60.

16. Chin SS, Lim TM, Chiang K, Fane AG. Factors affecting the performance of a low-pressure submerged membrane photocatalytic reactor. *Chem Eng J*. 2007; 130(1): 53-63.
17. Sakkas VA, Islam MA, Stalikas C, Albanis TA. Photocatalytic degradation using design of experiments: A review and example of the Congo red degradation. *J Hazard Mater*. 2010; 175(1-3): 33-44.
18. Pirkaram A, Olya ME, Farshid SR. UV/Ni-TiO₂ nanocatalyst for electrochemical. *Water Resours Ind*. 2014; 5: 9-20.
19. Zhang J, Fu D, Xu Y, Liu C. Optimization of parameters on photocatalytic degradation of chloramphenicol using TiO₂ as photocatalyst by response surface methodology. *J of Environ Sci*. 2010; 22(8): 1281-9.
20. Ferreir SLC, Bruns RE, Ferreira HS, Matos GD, David JM, Brandao GC, da Silva EGP, Portugal LA, dos Reis PS, Souza AS, dos Santos WNL. Box-Behnken design: an alternative for the optimization of analytical methods. *Anal Chim Acta*. 2007; 597(2): 179-186.
21. Ay F, Catalkaya EC, Kargi F. A statistical experiment design approach for advanced oxidation of Direct Red azo-dye by photo-Fenton treatment. *J Hazar Mater*. 2009; 162(1): 230-6.
22. Wang JP, Chen YZ, Wang Y, Yuan SJ, Yu HQ. Optimization of the coagulation-flocculation process for pulp mill wastewater treatment using a combination of uniform design and response surface methodology. *Water Research*. 2011; 45(17): 5633-40.
23. Zhou M, Yu J, Cheng B. Effects of Fe-doping on the photocatalytic activity of mesoporous TiO₂ powders prepared by an ultrasonic method. *J Hazar Mater*. 2006; 137(3): 1838-47.
24. Garcia, J. C., & Takashima, K. (). Photocatalytic degradation of imazaquin in an aqueous suspension of titanium dioxide. *Journal of Photochemistry and Photobiology A: Chemistry*. 2003; 155(1): 215-22.
25. Eslami, A., Nasser S, Yadollahi B, Mesdaghinia A, Vaezi F, Nabizadeh R, Nazmara S. Photocatalytic degradation of methyl tert-butyl ether (MTBE) in contaminated water by ZnO nanoparticles. *J Chem Technol Biotechnol*. 2008; 83(11): 1447-53.
26. Nikazar M, Gholivand K, Mahanpoor K. Photocatalytic degradation of azo dye Acid Red 114 in water with TiO₂ supported on clinoptilolite as a catalyst. *Desalination*. 2008; 219(1-3): 293-300.
27. Wang JP, Chen YZ, Wang Y, Yuan S, Yu HQ. Optimization of the coagulation-flocculation process for pulp mill wastewater treatment using a combination of uniform design and response surface methodology. *Water Research*. 2011; 45(17): 5633-40.
28. Zhang J, Fu D, Xu Y, Liu C. Optimization of parameters on Photocatalytic degradation of chloramphenicol using TiO₂ photocatalyst by response surface methodology. *J Environ Sci*. 2010; 12(8): 1281-9.
29. Ferreira SL, Bruns RE, Ferreira HS, Matos GD, David JM, Brandao GC, da Silva EG, Portugal LA, dos Reis PS, Souza AS, dos Santos WN. Box-Behnken design: an alternative for the optimization of analytical methods. *Anal Chim Acta*. 2007; 597(2): 179-86.
30. Tonga T, Zhanga J, Tiana B, Chena F, Heb D. Preparation of Fe³⁺-doped TiO₂ catalysts by controlled hydrolysis of titanium alkoxide and study on their Photocatalyticactivity for methyl orange degradation. *J Hazard Mater*. 2008; 155(3): 572-9.
31. Hu Q, Zhang C, Wang Z, Chen Y, Mao K, Zhang X, Xiong Y, Zhu M. Photodegradation of methyl tert-butyl ether (MTBE) by UV/H₂O₂ and

- UV/TiO₂. J Hazard Mater 2008; 154(1-3): 795–803.
32. Safari M, Nikazar M, Dadvar M. Photocatalytic degradation of methyl tert-butyl ether (MTBE) by Fe-TiO₂ nanoparticles. J Ind Eng Chem. 2013; 19(5): 1697–702.